

## Highly Conductive and Porous Lignin-derived Carbon Fibers

Guosheng Jia, Yan Yu, Xuefen Wang, Chao Jia \*, Zexu Hu, Senlong Yu, Hengxue Xiang \*,

Meifang Zhu

*State Key Laboratory for Modification of Chemical Fibers and Polymer Materials, College of Materials Science and Engineering, Donghua University, Shanghai 201620, China*

\*Corresponding author. Tel: +86 21 67792857; Fax: +86 21 67792855.

**Email:** jiachao0806@dhu.edu.cn; hengxuexiang@dhu.edu.cn

**Equations S1.** The bulk density of the LCFs.

**Equations S2.** The porosity of the LCFs.

**Equations S3.** The pore volume ( $V_{\text{pore}}$ ) of the LCFs.

**Equations S4.** The average pore diameter ( $D_{\text{pore}}$ ) of LCFs.

**Equations S5.** The area specific capacitance ( $C_{\text{electrode}}$ ) of the LCF-1500-based electrodes.

**Table S1.** Carbonization parameters of lignin carbon fibers (LCFs).

**Table S2.** Infrared spectral signal peaks of the LCFs and their assignments.

**Table S3.** Properties of LCFs obtained in the present study.

**Table S4.** Comparison of the specific surface area of the LCF-1500 with other reported carbon fibers.

**Table S5.** Fitted functions of structural and property parameters of the LCFs as a function of carbonization temperature (x).

**Table S6.** Comparison of the electrical conductivity of the LCFs with reported carbon materials.

**Table S7.** Performance comparison of the anodes based on the LCFs and other bio-based carbon materials.

**Fig. S1.** Large-scale preparation of lignin fibers.

**Fig. S2.** Effects of carbonization temperature on the morphology of the LCFs.

**Fig. S3.** Structure of the LCFs prepared at different carbonization temperatures.

**Fig. S4.** Structure and properties of the LCFs prepared at different carbonization temperatures.

**Fig. S5.** Effect of carbonization temperature on the elemental composition of the LCFs.

**Fig. S6.** Effect of carbonization heating rate on the morphology and structure of the LCFs.

**Fig. S7.** Specific surface area of the LCFs.

**Fig. S8.** La of the LCFs variation with carbonization temperature.

**Fig. S9.** Schematic diagram of the stacking arrangement of the graphite crystalline hexagonal carbon network.

**Fig. S10.** Performance of the LCF-based lithium-ion battery anodes.

**Fig. S11.** Morphology and elemental composition of LCF-1500-based electrode before and after cycling.

**Fig. S12.** Performance of the LCF-1500-based full cell.

**Fig. S13.** Performance of LCF-1500-based electrodes in supercapacitors.

## Structural characteristics of the LCFs

The bulk density, porosity, pore volume, and average pore diameter of the LCFs were calculated using Equations S1-S4 as outlined below:

- The bulk density of the LCFs ( $\rho_L$ ) was calculated using Equation S1:

$$\rho_L = \frac{m}{V} \quad (\text{Equation S1})$$

where m and V are the weight and the volume of the LCFs, which were measured by digital balance and vernier caliper, respectively.

- The porosity of the LCFs was calculated using Equation S2:

$$\text{Porosity}[\%] = \left(1 - \frac{\rho_L}{\rho_C}\right) \quad (\text{Equation S2})$$

$\rho_C$  is the physical density of carbon (1.8 g cm<sup>-3</sup>).

- The pore volume ( $V_{pore}$ ) and average pore diameter ( $D_{pore}$ ) were calculated using Equation S3 and S4, respectively<sup>2</sup>:

$$V_{pore} = \frac{1}{\rho_L} - \frac{1}{\rho_C} \quad (\text{Equation S3})$$

$$D_{pore} = \frac{4V_{pore}}{A} \quad (\text{Equation S4})$$

where A is the specific surface area obtained from nitrogen adsorption-desorption isotherms.

## Performance of the LCF-1500 in supercapacitors

The area specific capacitance ( $C_{electrode}$ ) of the electrodes was obtained from the Galvanostatic charge/discharge (GCD) curves of the three-electrode system by Equation S5:

$$C_{electrode} = \frac{(\Delta t \times I)}{A \times \Delta U} \quad (\text{Equation S5})$$

where  $\Delta t$  and I are the discharge time and the discharge current, respectively, and A and  $\Delta U$  are

the electrode's working area and potential window, respectively.

**Table S1.** Carbonization parameters of lignin carbon fibers (LCFs).

Samples	Carbonization temperature (°C)	Heating rate (°C min <sup>-1</sup> )
LCF-900	900	3
LCF-1100	1100	3
LCF-1300	1300	3
LCF-1500	1500	3
LCF-2000	2000	3
LCF-2400	2400	3
LCF-2800	2800	3
LCF-1500-2	1500	2
LCF-1500-4	1500	4
LCF-1500-5	1500	5

**Table S2.** Infrared spectral signal peaks of the LCFs and their assignments.

Wavenumber (cm <sup>-1</sup> )	Assignments
3440	O-H stretching (Hydrogen-bonded)
2907	C-H stretching in O-CH <sub>3</sub> , asymmetric
2837	C-H stretching in O-CH <sub>3</sub> , symmetric
1630	C=C stretching vibration
1380	C-H bending vibration
1100	C-O stretching vibration

**Table S3.** Properties of LCFs obtained in the present study.

	V <sub>pore</sub> (cm <sup>3</sup> g <sup>-1</sup> )	D <sub>pore</sub> (nm)	Porosity (%)	SSA (m <sup>2</sup> g <sup>-1</sup> )
LCF-900	0.276	61.4	33.2	18
LCF-1100	1.79	31.9	76.3	225
LCF-1300	2.98	16.1	83.9	721
LCF-1500	3.51	15.2	86.3	923
LCF-2000	0.405	35.2	42.1	46

**Table S4.** Comparison of the specific surface area of the LCF-1500 with other reported carbon fibers.

Type of carbon fibers	Fiber preparation method	Activation method	Specific surface area ( $\text{m}^2 \text{ g}^{-1}$ )	Reference
LCF-1500	Melt-blown	-	$923 \pm 47$	This work
Polyacrylonitrile (PAN) activated carbon nanofibers (ACNF)	Electrospinning	CO	705	<sup>3</sup>
Lignin/polyvinylpyrrolidone (PVP) carbon nanofiber (CNF)	Electrospinning	-	600	<sup>4</sup>
Lignin/ polyvinyl alcohol (PVA) CNF	Electrospinning	-	583	<sup>5</sup>
Lignin/ polyethylene oxide (PEO) carbon fiber (CF)	Electrospinning	-	456	<sup>6</sup>
Cellulose CNF	Extraction from cellulose	-	300.2	<sup>7</sup>

PAN/ PVP activated carbon fibers (ACF)	Solution spinning	Hydrazine hydrate	277.4	8
PAN/ poly(methylmethacrylate) (PMMA) CF	Electrospinning	-	94	9
Alkali lignin (AL) derived ACF	Electrospinning	H <sub>2</sub> SO <sub>4</sub>	85.67	10
Acetic anhydride (AA) modified LCF	Melt spinning	-	37.4	11
AL derived CF	Electrospinning	-	33.89	10
Phthalic anhydride (PA) modified LCF	Melt spinning	-	32.72	11
Succinic anhydride (SA) modified LCF	Melt spinning	-	15.32	11
Unmodified LCF	Melt spinning	-	8.20	11
Maleic anhydride (MA) modified LCF	Melt spinning	-	6.39	11

**Table S5.** Fitted functions of structural and property parameters of the LCFs as a function of carbonization temperature (x).

Parameters (y)	Equation	a	b	c	R <sup>2</sup>
I <sub>G</sub> /I <sub>D</sub>	y = a*(1 - exp(-b*x))	-0.090 ± 0.045	-0.001 ± 1.864E-4	-	0.96428
Electrical conductivity	y = a + b*x	-4.170 ± 0.678	0.005 ± 3.696E-4	-	0.9713
La	y = a + b*x <sup>1</sup> + c*x <sup>2</sup>	21.206 ± 5.682	-0.025 ± 0.007	8.369E-6 ± 1.835E-6	0.94118
Lc	y = (a/(a-b))*(exp(-b*x) - exp(-a*x))	4.375E-4 ± 2.428E-4	-0.001 ± 2.020E-4	-	0.95308
d <sub>002</sub>	Y = 0.339 + (a/(b*sqrt(pi/2)))*exp(-2*((x-c)/b) <sup>2</sup> )	51.686 ± 12.133	968.039 ± 197.847	1046.843 ± 77.503	0.96902

**Table S6.** Comparison of the electrical conductivity of the LCFs with reported carbon materials.

Carbon materials	Carbonization temperature (°C)	Fiber preparation method	Applications	Electrical conductivity (S cm <sup>-1</sup> )	Reference
LCF-2800	2800	Melt-blown	Lithium-ion battery electrodes	714	This work
LCF-2400	2400	Melt-blown	Unexplored	166	This work
LCF-2000	2000	Melt-blown	Unexplored	10	This work
LCF-1500	1500	Melt-blown	Lithium-ion battery electrodes	4.13	This work
LCF-1300	1300	Melt-blown	Unexplored	1.68	This work
LCF-1100	1100	Melt-blown	Lithium-ion battery electrodes	0.55	This work
LCF-900	900	Melt-blown	Unexplored	0.344	This work

Cotton based carbon	800	Cotton natural fiber	Cell proliferation and differentiation	0.33	<a href="#">12</a>
Kraft lignin based CF	1000	Electrostatic spinning	Unexplored	19.6	<a href="#">13</a>
Cellulose based CF	800	Electrostatic spinning	Supercapacitor	10.2	<a href="#">14</a>
Bamboo based CF	3000	Extracted from bamboo fiber	Diffusion layer (GDL) of proton exchange membrane	550	<a href="#">15</a>
Lignin/PAN based CF	1400	Electrostatic spinning	Unexplored	21.3	<a href="#">16</a>
Corn stover lignin based CF	1000	Wet spinning	Unexplored	64.85	<a href="#">17</a>
Switchgrass lignin based CF	1000	Wet spinning	Unexplored	94	<a href="#">17</a>

Cellulose derived CF	600	Electrospinning	Unexplored	0.16	<a href="#">18</a>
Pine lignin based CF	1000	Wet spinning	Unexplored	130.71	<a href="#">17</a>
Red cedar based CF	1000	Wet spinning	Unexplored	139.09	<a href="#">17</a>
Sugar maple lignin based CF	1000	Wet spinning	Unexplored	142.25	<a href="#">17</a>
Lignin (SKL) based CF	1700	Melt spinning	Lithium-ion battery electrodes	191	<a href="#">19</a>
T300	1100-2000	Wet spinning	Commercial production	588	<a href="#">20</a>

---

**Table S7.** Performance comparison of the anodes based on the LCFs and other bio-based carbon materials.

Anode materials	Specific capacity (mAh g <sup>-1</sup> )	Number of cycles	Cycling rate (A g <sup>-1</sup> )	Retention (%)	Mass loading (mg cm <sup>-2</sup> )	Reference
LCF-1500	466	800	0.5 (~1 C)	71.9	1.69	This work
Softwood-derived biographite (a)	335	89	0.1 C	100	3.5	21
Lignin carbon nanofiber (b)	274	200	0.1 (~0.36 C)	75.4	1.04	22
Hazelnut shell-derived carbon (c)	307	100	1 C	59.8	-	23
Walnut shell-derived CNFs (d)	380	200	0.03 (~0.07 C)	90	3	24
Walnut shell-derived CNFs (e)	150	100	0.1 (~0.67C)	99.5	4	25
Loofah-derived carbon (f)	225	200	0.1 (~0.5C)	90	1.0–2.0	26

Sisal fiber-derived carbon (g)	250	30	0.1 C	85	-	<a href="#">27</a>
Rice husk-derived carbon (h)	403	100	0.075 (~0.2 C)	-	-	<a href="#">28</a>
Mushroom-derived carbon (i)	260	700	0.2C	-	1	<a href="#">29</a>
Coffee shell-derived carbon (j)	200	15	0.2C	50	-	<a href="#">30</a>
Rice husk-derived carbon (k)	354	10	0.1C	76	-	<a href="#">31</a>
Pine cone shell-derived carbon (l)	394	8	0.01 (~0.02 C)	-	-	<a href="#">32</a>
Peanut shell-derived carbon (m)	325	70	0.1C	-	-	<a href="#">33</a>
Sterculia scaphigera-derived carbon (n)	423	100	0.1 C	70.5	1	<a href="#">34</a>
Potato-derived carbon (o)	531	20	0.1C	93	-	<a href="#">35</a>
Sweet potato-derived carbon (p)	300	200	0.1 (~0.33 C)	99	-	<a href="#">36</a>

Bamboo chopsticks-derived carbon (q)	360	800	0.37 C	-	2.5–4.0	<a href="#">37</a>
Glucose with chestnut shell-derived carbon (r)	411	100	0.1 (~0.25C)	<50	-	<a href="#">38</a>
Eggshell film-derived carbon (s)	300	300	0.2 (~0.67C)	72	-	<a href="#">39</a>
Algae-derived carbon (t)	443	500	0.1C	97.4	-	<a href="#">40</a>

---

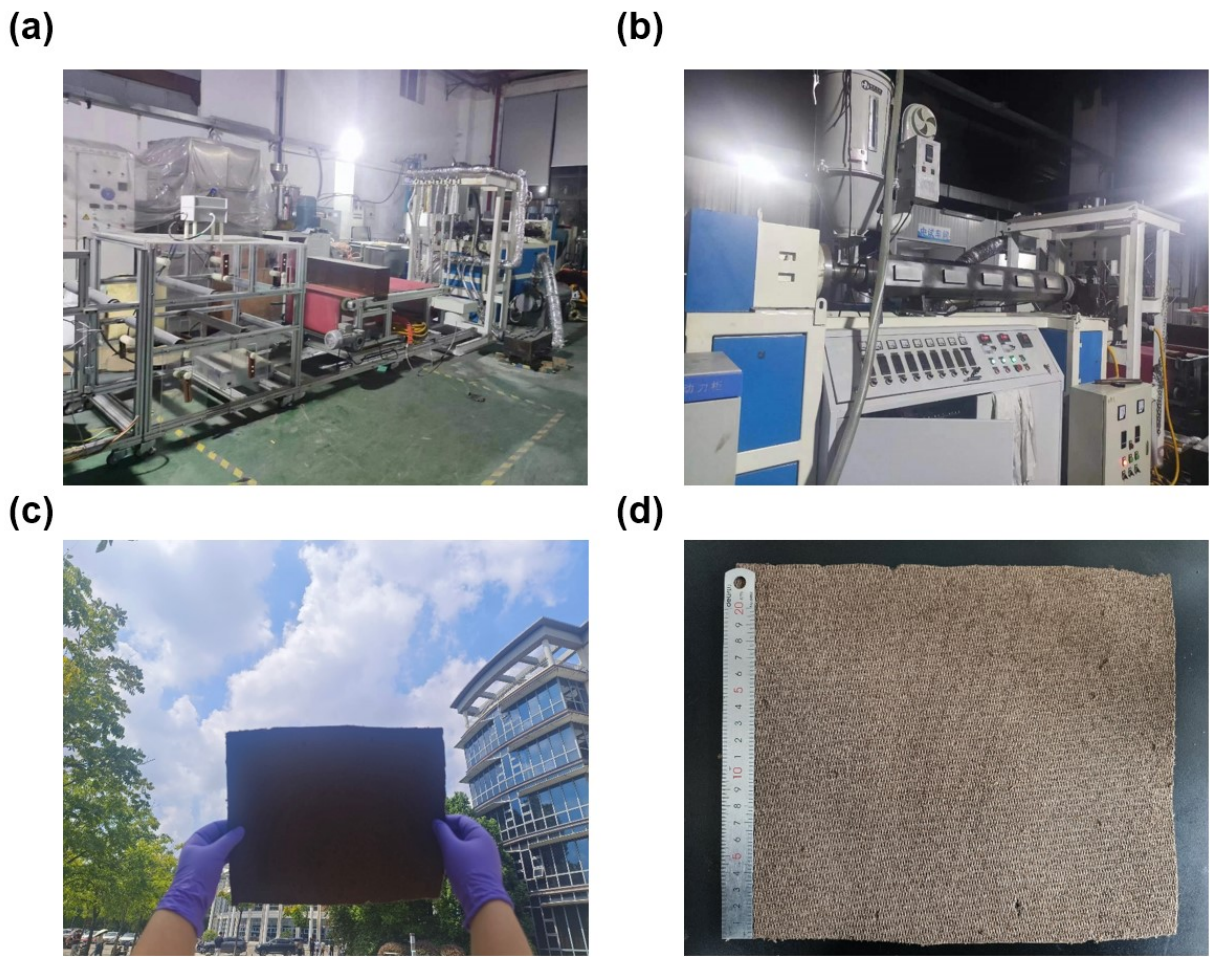


**Fig. S1.** Large-scale preparation of lignin fibers. Digital images of (a, b) melt blowing machine, and (c, d) lignin fiber mat.

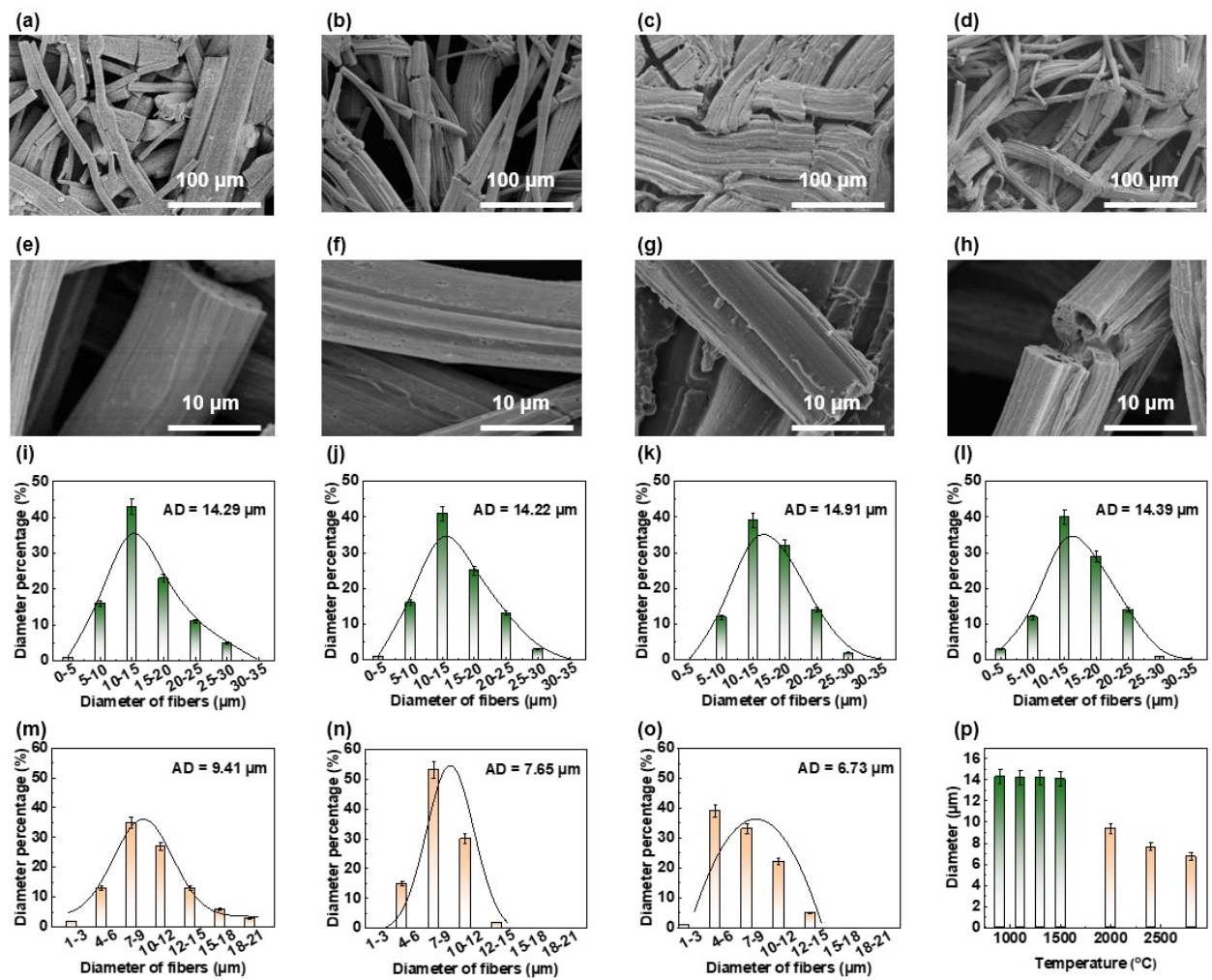


**Fig. S2.** Effects of carbonization temperature on the morphology of the LCFs. SEM images of the LCFs prepared at carbonization temperature of (a, e) 1100°C, (b, f) 1300°C, (c, g) 2000°C, (d, h) 2400°C. Diameter distribution histograms of the LCFs prepared at carbonization temperature of (i) 900°C, (j) 1100°C, (k) 1300°C, (l) 1500°C, (m) 2000°C, (n) 2400°C, (o) 2800°C. (p) Histogram of the average diameter of the LCFs.

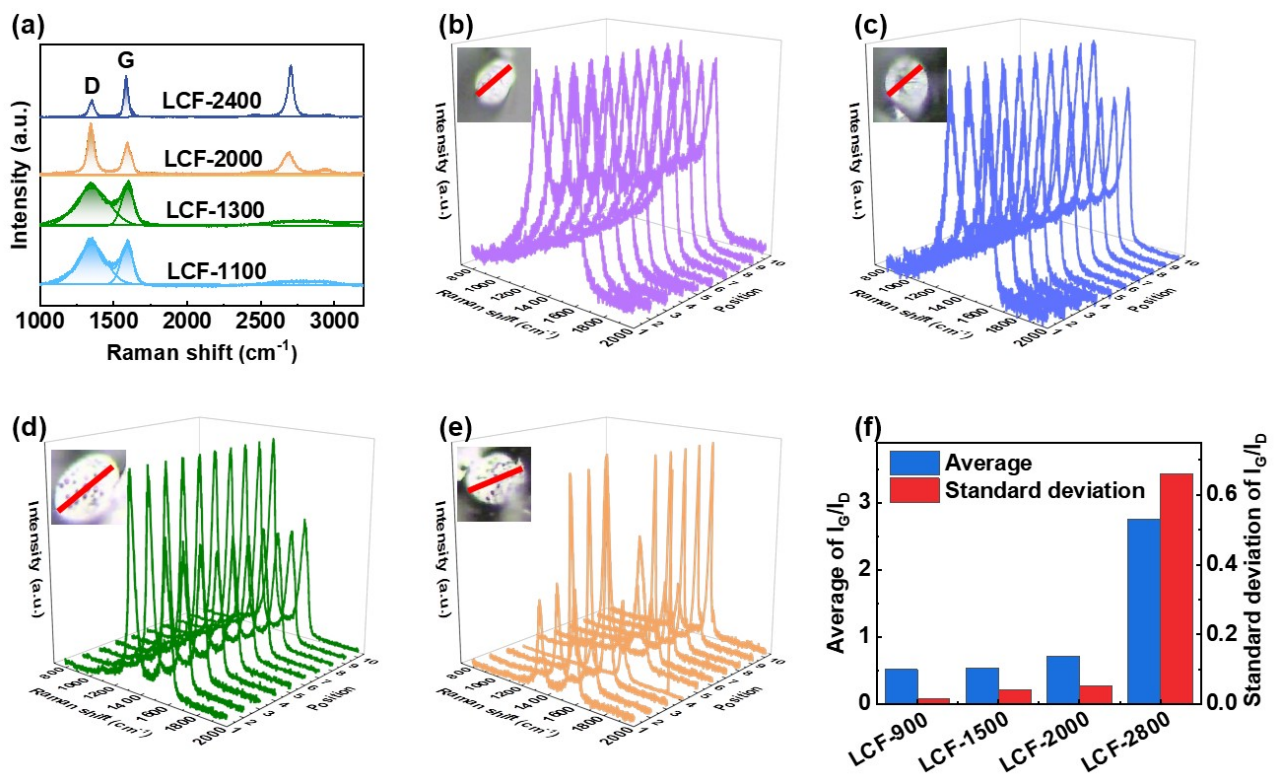


**Fig. S3.** Structure of the LCFs prepared at different carbonization temperatures. (a) Raman spectra of the LCFs. Radial structure of the LCFs: (b) LCF-900, (c) LCF-1500, (d) LCF-2000, (e) LCF-2800, (f) Average and standard deviation of  $I_G/I_D$  of LCFs.

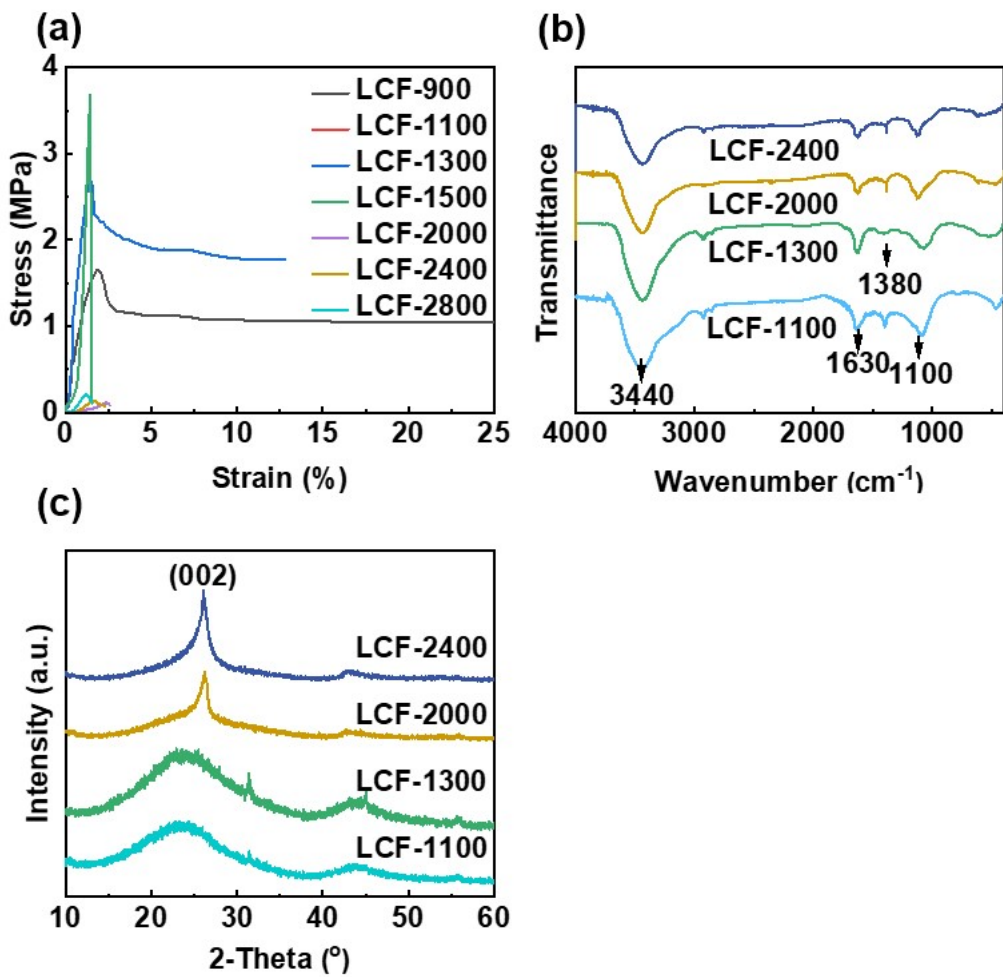


**Fig. S4.** Structure and properties of the LCFs prepared at different carbonization temperatures. (a) Stress-strain curves of the LCFs. (b) FTIR spectra and (c) XRD patterns of the LCFs.

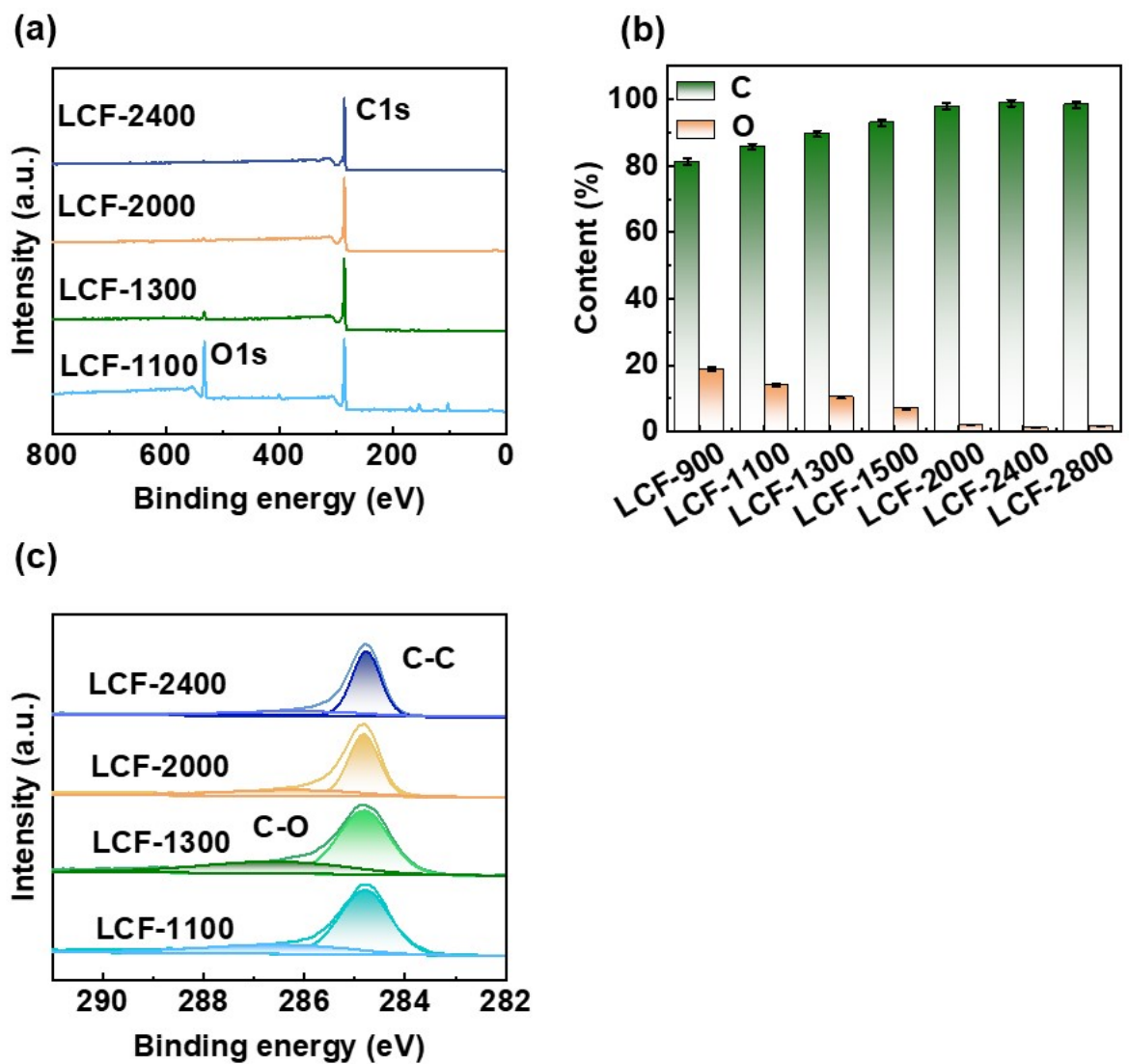


**Fig. S5.** Effect of carbonization temperature on the elemental composition of the LCFs. (a) XPS spectra and (b) elemental content of the LCFs. (c) XPS C1s spectra of the LCFs.

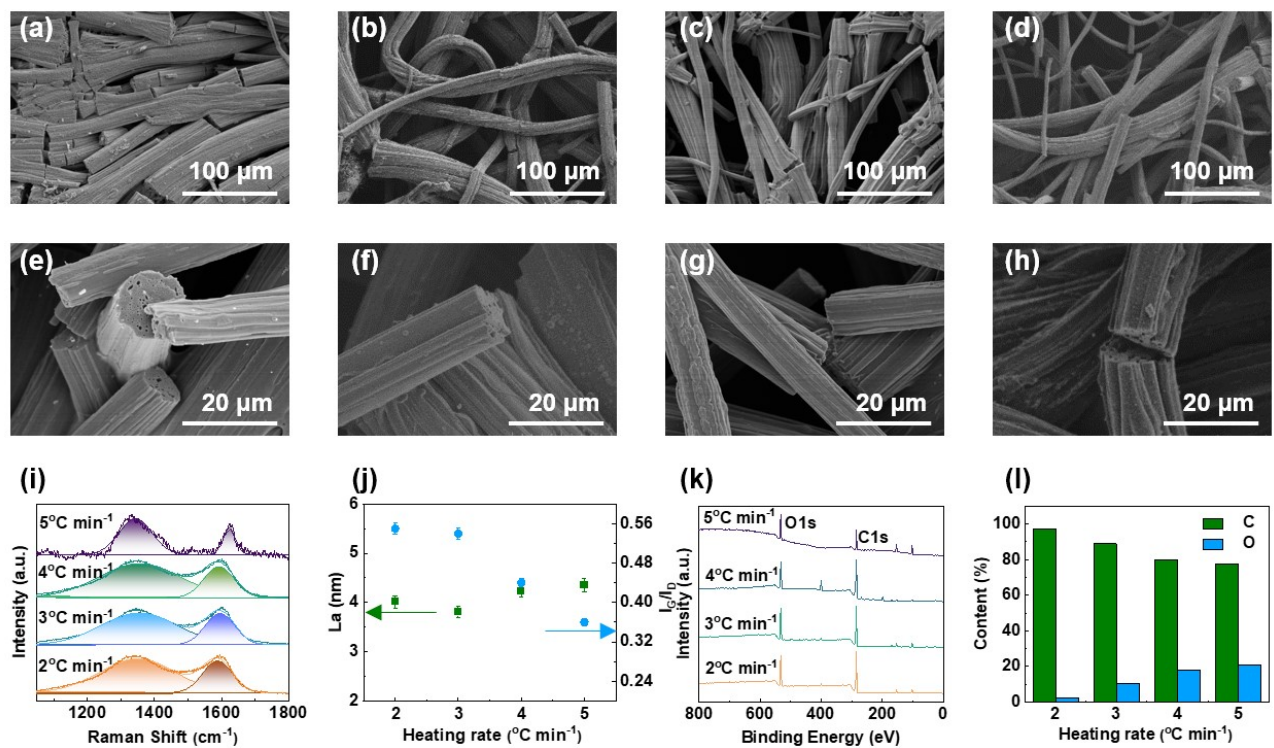


**Fig. S6.** Effect of carbonization heating rate on the morphology and structure of the LCFs. SEM images of the LCFs prepared at carbonization heating rate of (a, e)  $2^{\circ}\text{C min}^{-1}$ , (b, f)  $3^{\circ}\text{C min}^{-1}$ , (c, g)  $4^{\circ}\text{C min}^{-1}$ , (d, h)  $5^{\circ}\text{C min}^{-1}$ . (i) Raman spectra, (j) La and  $I_G/I_D$ , (k) XPS spectra, (l) elemental content of the LCFs.

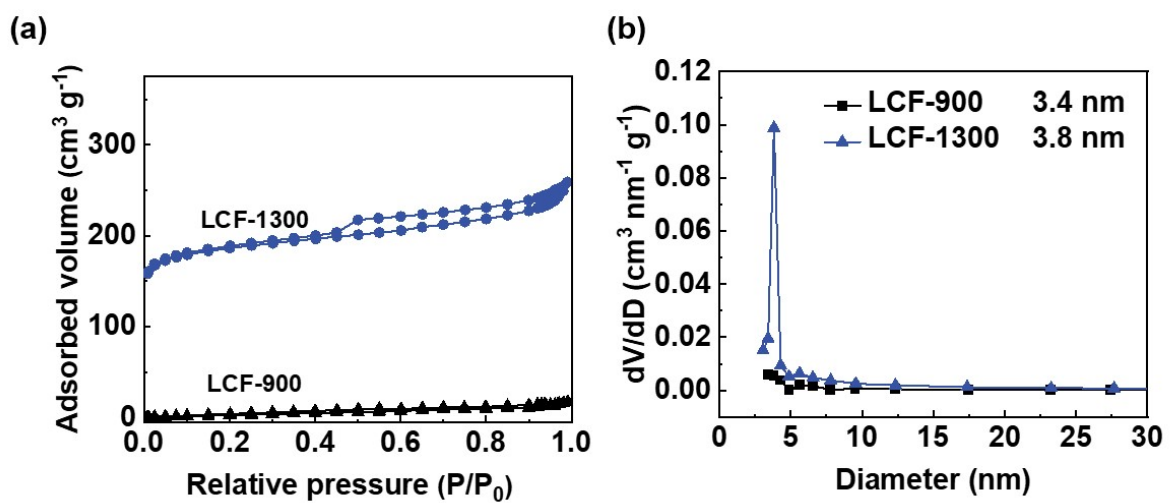


**Fig. S7.** Specific surface area of the LCFs. (a) Nitrogen adsorption isotherms and (b) pore size distribution of the LCFs.

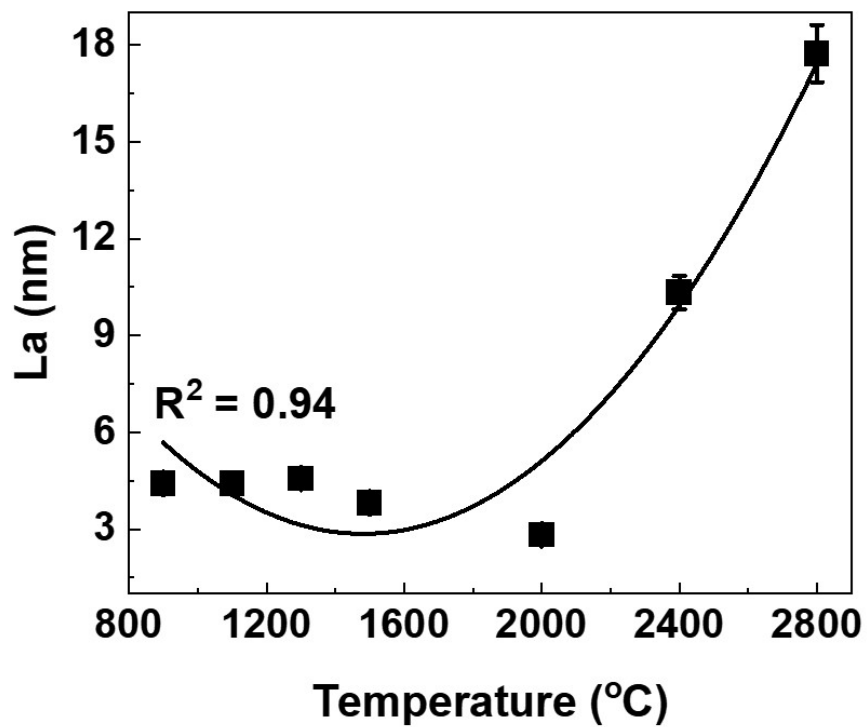


**Fig. S8.**  $La$  of the LCFs variation with carbonization temperature.

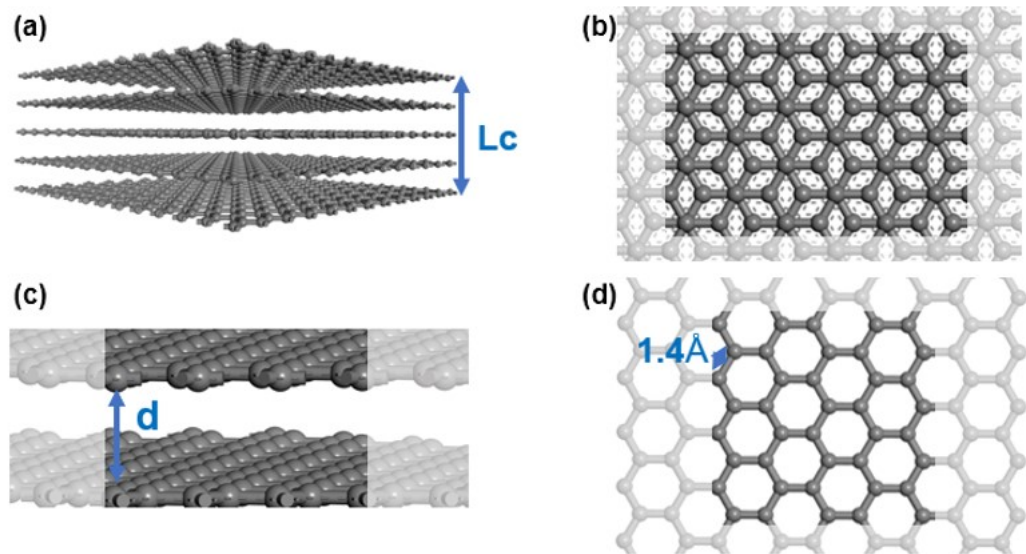


**Fig. S9.** Schematic diagram of the stacking arrangement of the graphite crystalline hexagonal carbon network. (a) Main view. (b) Top view. (c) Enlarged side view. (d) Top view of a single graphite sheet.

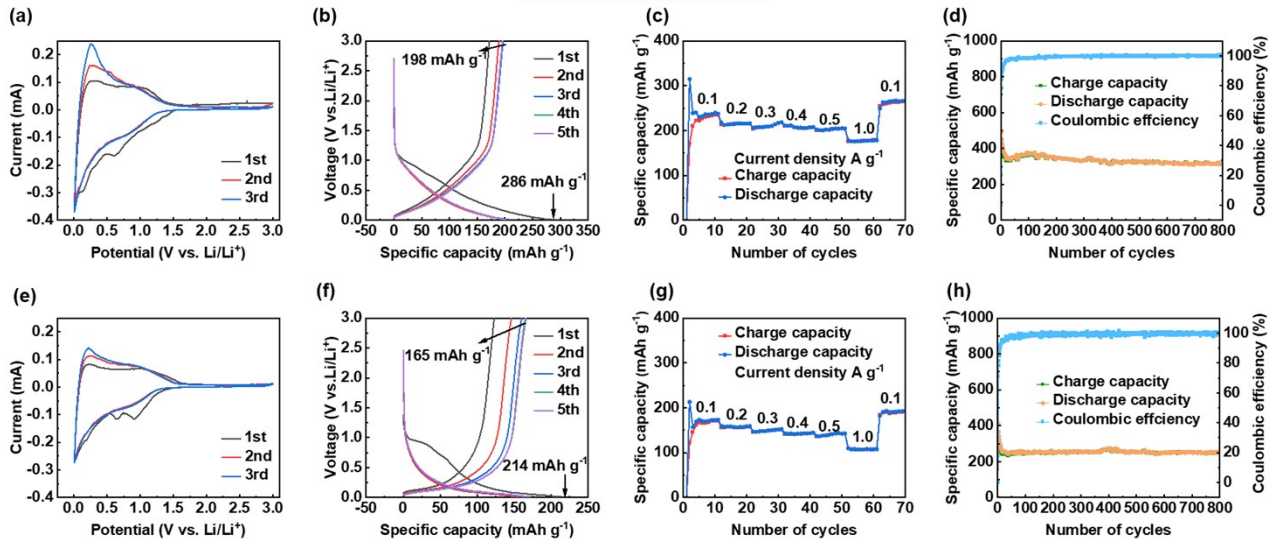


**Fig. S10.** Performance of the LCF-based lithium-ion battery anodes. (a) CV curves, (b) charge/discharge profiles, (c) rate capabilities at various current densities, and (d) long-term charge-discharge behavior of the assembled lithium-ion battery anodes based on LCF-1100. (e) CV curves, (f) charge/discharge profiles, (g) rate capabilities at various current densities, and (h) long-term charge-discharge behavior of the assembled lithium-ion battery anodes based on LCF-2800.

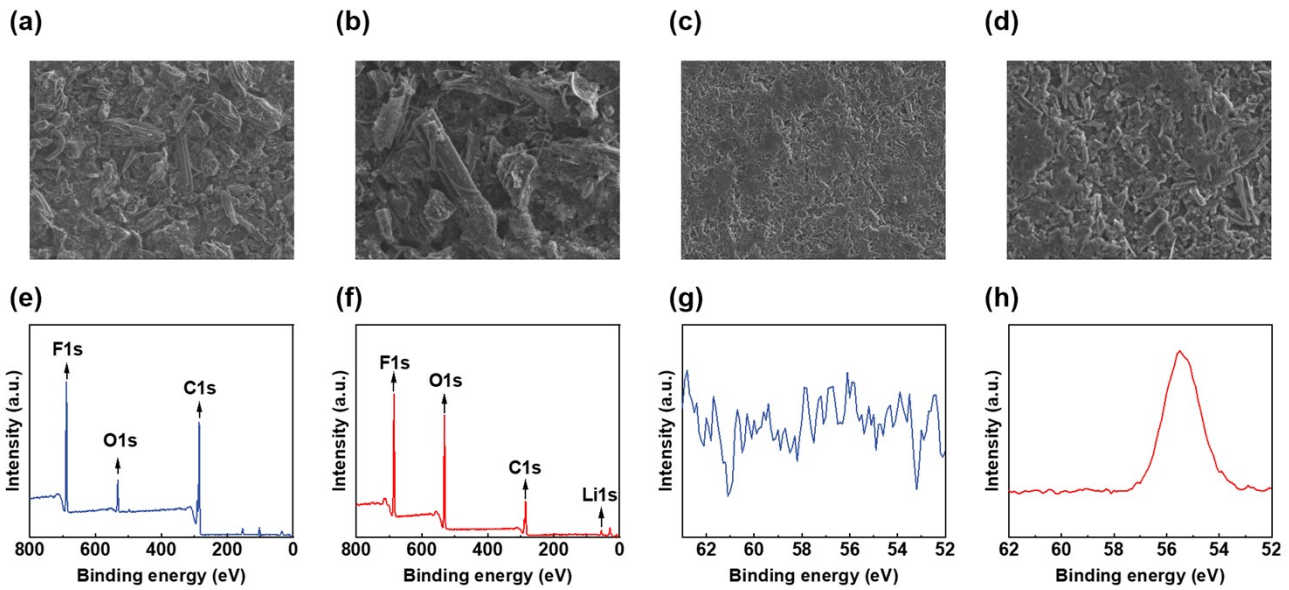


**Fig. S11.** Morphology and elemental composition of LCF-1500-based electrode before and after cycling. SEM images of LCF-1500-based electrode (a, b) before cycling and (c, d) after cycling. XPS spectra of LCF-1500-based electrode (e) before cycling and (f) after cycling. XPS Li1s spectra of LCF-1500-based electrode (g) before cycling and (h) after cycling.

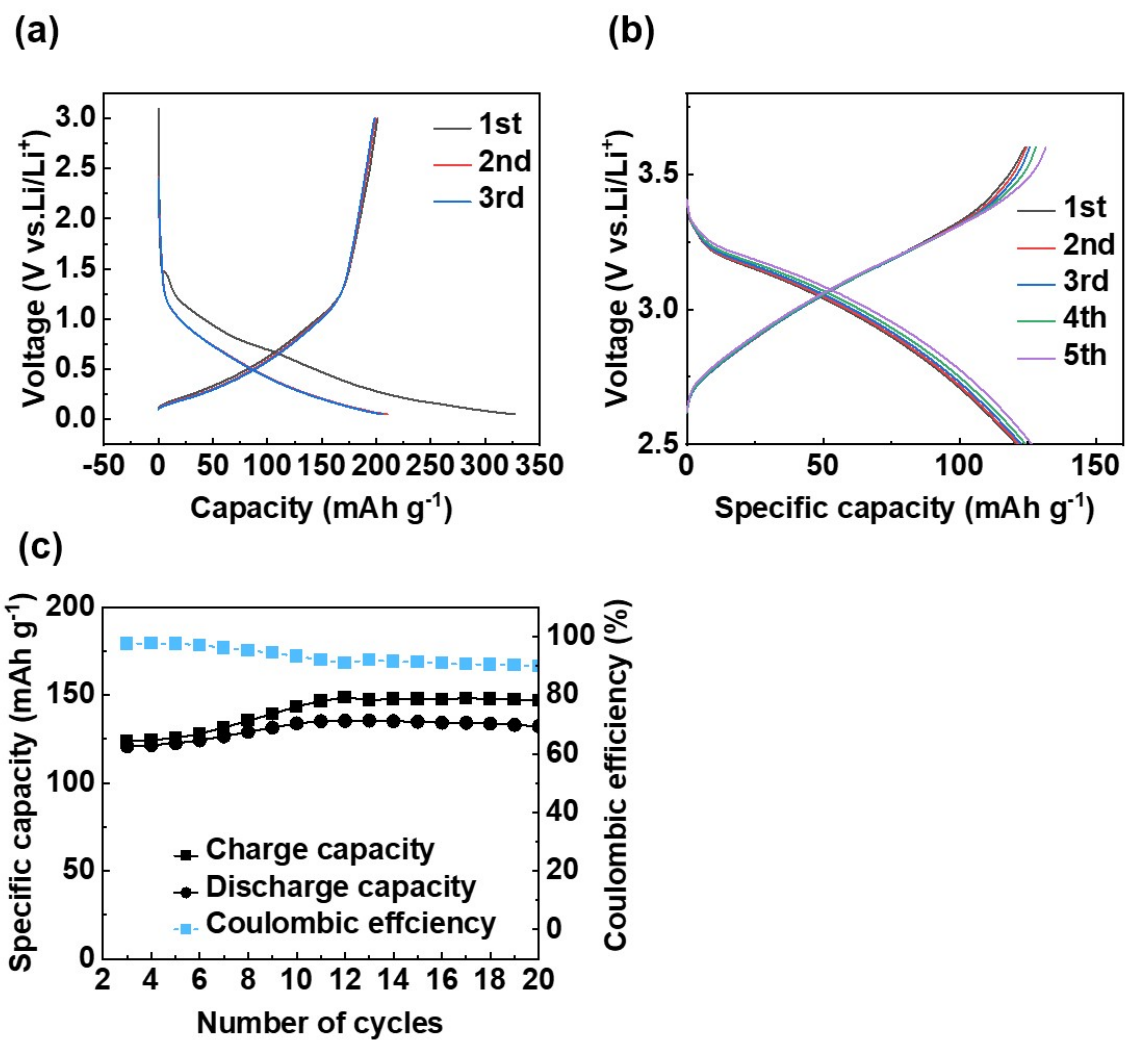


**Fig. S12.** Performance of the LCF-1500-based full cell. (a) GCD curves for pre-lithiation of the LCF-1500-based electrodes. (b) GCD curves and (c) long-term charge-discharge behavior recorded at 0.1 C for the LCF-1500-based full cell.

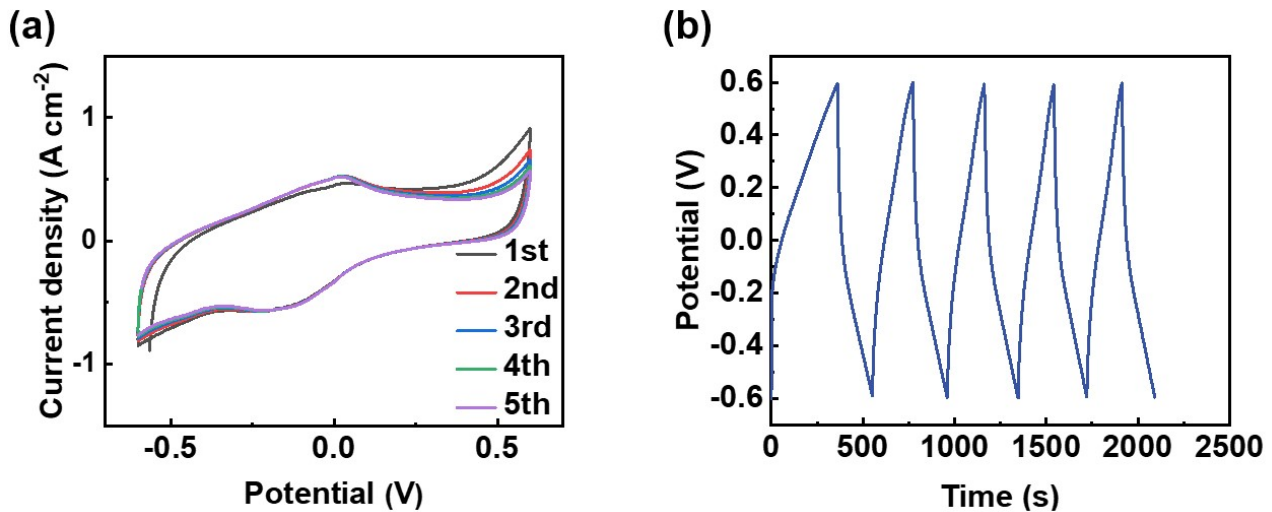


**Fig. S13.** Performance of LCF-1500-based electrodes in supercapacitors. (a) CV profiles collected at  $10 \text{ mV s}^{-1}$ , and (b) GCD curves recorded at  $2 \text{ mA cm}^{-2}$ .

## References

1. H. G. Chae, B. A. Newcomb, P. V. Gulgulje, Y. Liu, K. K. Gupta, M. G. Kamath, K. M. Lyons, S. Ghoshal, C. Pramanik, L. Giannuzzi, K. Şahin, I. Chasiotis and S. Kumar, *Carbon*, 2015, **93**, 81-87.
2. J. Zhang, Y. Cheng, M. Tebyetekerwa, S. Meng, M. Zhu and Y. Lu, *Adv. Funct. Mater.*, 2019, **29**, 1806407.
3. E. J. Ra, E. Raymundo-Piñero, Y. H. Lee and F. Béguin, *Carbon*, 2009, **47**, 2984-2992.
4. C. Ma, Z. Li, J. Li, Q. Fan, L. Wu, J. Shi and Y. Song, *Appl. Surf. Sci.*, 2018, **456**, 568-576.
5. C. Lai, Z. Zhou, L. Zhang, X. Wang, Q. Zhou, Y. Zhao, Y. Wang, X.-F. Wu, Z. Zhu and H. Fong, *J. Power Sources*, 2014, **247**, 134-141.
6. I. Dallmeyer, L. T. Lin, Y. Li, F. Ko and J. F. Kadla, *Macromol. Mater. Eng.*, 2014, **299**, 540-551.
7. Z. Zhang, J. Zhang, X. Zhao and F. Yang, *Carbon*, 2015, **95**, 552-559.
8. L. Li, X.-F. Wang, J.-J. Zhong, X. Qian, S.-L. Song, Y.-G. Zhang and D.-H. Li, *Ind. Eng. Chem. Res.*, 2018, **57**, 11608-11616.
9. C.-C. Lai and C.-T. Lo, *Electrochim. Acta*, 2015, **183**, 85-93.
10. T. Worarutariyachai and S. Chuangchote, *BioResources*, 2020, **15**, 2.
11. S. Chatterjee and T. Saito, *ChemSusChem*, 2015, **8**, 3941-3958.
12. X. Chen, Y. Wu, V. D. Ranjan and Y. Zhang, *Carbon*, 2018, **134**, 174-182.
13. I. Dallmeyer, L. T. Lin, Y. Li, F. Ko and J. F. Kadla, *Macromol. Mater. Eng.*, 2014, **299**, 540-551.
14. V. Kuzmenko, O. Naboka, H. Staaf, M. Haque, G. Göransson, P. Lundgren, P. Gatenholm and P. Enoksson, *Mater. Chem. Phys.*, 2015, **160**, 59-65.
15. T. Kinumoto, T. Matsumura, K. Yamaguchi, M. Matsuoka, T. Tsumura and M. Toyoda, *ACS Sustainable Chem. Eng.*, 2015, **3**, 1374-1380.

16. W.-J. Youe, S.-M. Lee, S.-S. Lee, S.-H. Lee and Y. S. Kim, *Int. J. Biol. Macromol.*, 2016, **82**, 497-504.
17. Q. Li, C. Hu, M. Li, P. Truong, J. Li, H.-S. Lin, M. T. Naik, S. Xiang, B. E. Jackson and W. Kuo, *Green Chem.*, 2021, **23**, 3725-3739.
18. H. Gaminian and M. Montazer, *Cellulose*, 2018, **25**, 5227-5240.
19. A. P. Nowak, J. Hagberg, S. Leijonmarck, H. Schweinebarth, D. Baker, A. Uhlin, P. Tomani and G. Lindbergh, *Holzforschung*, 2018, **72**, 81-90.
20. Y. Liu and S. Kumar, *Polym. Rev.*, 2012, **52**, 234-258.
21. W. J. Sagues, J. Yang, N. Monroe, S.-D. Han, T. Vinzant, M. Yung, H. Jameel, M. Nimlos and S. Park, *Green Chem.*, 2020, **22**, 7093-7108.
22. M. Culebras, G. A. Collins, A. Beaucamp, H. Geaney and M. N. Collins, *Eng. Sci.*, 2022, **17**, 195-203.
23. E. Unur, S. Brutti, S. Panero and B. Scrosati, *Microporous Mesoporous Mater.*, 2013, **174**, 25-33.
24. L. Tao, Y. Huang, Y. Zheng, X. Yang, C. Liu, M. Di, S. Larpkiattaworn, M. R. Nimlos and Z. Zheng, *J. Taiwan Inst. Chem. Eng.*, 2019, **95**, 217-226.
25. L. Tao, Y. Zheng, Y. Zhang, H. Ma, M. Di and Z. Zheng, *RSC Adv.*, 2017, **7**, 27113-27120.
26. Z. Wu, L. Wang, J. Huang, J. Zou, S. Chen, H. Cheng, C. Jiang, P. Gao and X. Niu, *Electrochim. Acta*, 2019, **306**, 446-453.
27. X. Yu, K. Zhang, N. Tian, A. Qin, L. Liao, R. Du and C. Wei, *Mater. Lett.*, 2015, **142**, 193-196.
28. L. Wang, Z. Schnepf and M. M. Titirici, *J. Mater. Chem. A*, 2013, **1**, 5269-5273.
29. B. Campbell, R. Ionescu, Z. Favors, C. S. Ozkan and M. Ozkan, *Sci. Rep.*, 2015, **5**, 14575.
30. Y. J. Hwang, S. K. Jeong, K. S. Nahm, J. S. Shin and A. Manuel Stephan, *J. Phys. Chem. Solids*, 2007, **68**, 182-188.
31. G. T.-K. Fey, Y.-D. Cho, C.-L. Chen, Y.-Y. Lin, T. P. Kumar and S.-H. Chan, *Pure Appl. Chem.*, 2010, **82**, 2157-2165.

32. Y. Zhang, F. Zhang, G.-D. Li and J.-S. Chen, *Mater. Lett.*, 2007, **61**, 5209-5212.
33. G. T. K. Fey, Y. Y. Lin, K. P. Huang, Y. C. Lin, T. P. Kumar, Y. D. Cho and H. M. Kao, *Adv. Mater. Res.*, 2011, **415-417**, 1572-1585.
34. W. Wang, Y. Wan, S. Wu, M. Li, L. Cao, F. Lv, M. Yang, Z. Sun, R. Sun and Z. Lu, *RSC Adv.*, 2015, **5**, 46558-46563.
35. W. Li, M. Chen and C. Wang, *Mater. Lett.*, 2011, **65**, 3368-3370.
36. P. Zheng, T. Liu, J. Zhang, L. Zhang, Y. Liu, J. Huang and S. Guo, *RSC Adv.*, 2015, **5**, 40737-40741.
37. J. Jiang, J. Zhu, W. Ai, Z. Fan, X. Shen, C. Zou, J. Liu, H. Zhang and T. Yu, *Energy Environ. Sci.*, 2014, **7**, 2670-2679.
38. G. Xia, X. Li, J. He, Y. Wang, Y. Gu, L. Liu, J. Huang, P. Dong, J. Duan, D. Wang, Y. Zhang and Y. Zhang, *Ceram. Int.*, 2021, **47**, 20948-20955.
39. J. Zhao, J. A. Syed, X. Wen, H. Lu and X. Meng, *J. Alloys Compd.*, 2019, **777**, 974-981.
40. H. Ru, N. Bai, K. Xiang, W. Zhou, H. Chen and X. S. Zhao, *Electrochim. Acta*, 2016, **194**, 10-16.